© 2020. Published by The Company of Biologists Ltd | Journal of Cell Science (2020) 133, jcs239244. doi:10.1242/jcs.239244

RESEARCH ARTICLE

A novel benzodiazepine derivative that suppresses microtubule dynamics and impairs mitotic progression

Vittoria Pirani[1,2], Mathieu Métivier[1], Emmanuel Gallaud[1], Alexandre Thomas[1], Siou Ku[1], Denis Chretien[1], Roberta Ettari[3], Regis Giet[1,*], Lorenzo Corsi[2,*] and Christelle Benaud[1,*]

ABSTRACT

A novel 2,3-benzodiazepine-4 derivative, named 1*g*, has recently been shown to function as an anti-proliferative compound. We now show that it perturbs the formation of a functional mitotic spindle, inducing a spindle assembly checkpoint (SAC)-dependent arrest in human cells. Live analysis of individual microtubules indicates that 1*g* promotes a rapid and reversible reduction in microtubule growth. Unlike most anti-mitotic compounds, we found that 1*g* does not interfere directly with tubulin or perturb microtubule assembly *in vitro*. The observation that 1*g* also triggers a SAC-dependent mitotic delay associated with chromosome segregation in *Drosophila* neural stem cells, suggests that it targets a conserved microtubule regulation module in humans and flies. Altogether, our results indicate that 1*g* is a novel promising anti-mitotic drug with the unique properties of altering microtubule growth and mitotic spindle organization.

KEY WORDS: Microtubules, Mitosis, Anti-mitotic drug, Microtubule dynamics, SAC

INTRODUCTION

Microtubules are composed of α- and β-tubulin heterodimers whose assembly undergoes stochastic phases of growth and shrinkage in a process called dynamic instability (Mitchison and Kirschner, 1984). The microtubule network serves diverse and specific functions in differentiated cells such as scaffold and cargo transport. As the cell proceeds through mitosis, the microtubule network undergoes a dramatic reorganization to build a mitotic spindle used to equally segregate chromatids in the two daughter cells. *In vivo*, microtubule nucleation and organization, as well as their intrinsic dynamic instability, are regulated by microtubule-associated proteins (MAPs). The influence of MAPs on the dynamic assembly of microtubules contributes to the microtubule assembly patterns required for the proper formation of the mitotic spindle (Desai and Mitchison, 1997; Prosser and Pelletier, 2017).

The dynamic properties of mitotic spindle microtubules are required for fast and amphitelic attachment of sister kinetochores to the opposite spindle poles, an event essential to avoid mis-segregation of chromatids during anaphase and subsequent aneuploidy. In case of erroneous attachments of chromosomes to spindle microtubules, the spindle assembly checkpoint (SAC) remains unsatisfied and inhibits anaphase onset through inhibition of the anaphase promoting complex/cyclosome (APC/C). Cells are then delayed in mitosis until all defective attachments have been corrected (Khodjakov and Rieder, 2009).

The central role of microtubules in orchestrating cell division, together with the property of SAC-dependent mitotic delay, have made microtubules a target of choice for cancer chemotherapeutic agents aiming to block cell division (Janssen and Medema, 2011). Microtubule-binding compounds that block microtubule dynamics, such as Vinka alkaloid and taxanes, have emerged as efficient anti-tumor agents and are currently used in therapeutic treatments (Dumontet and Jordan, 2010). However, their use leads to severe side effects, including neuropathy (Argyriou et al., 2012). Moreover, a variability in the response to the treatment with these compounds in different tumor types is observed (Kavallaris, 2010). The identification of new anti-mitotic drugs with alternative modes of action thus remains a priority for anti-cancer research (Dumontet and Jordan, 2010).

Activation of the AMPA receptor by glutamate has long been known to enhance cell proliferation (Stepulak et al., 2014). A recent screen to identify new anti-proliferative compounds has highlighted the non-competitive AMPA receptor agonist derivate 1-(4-amino-3, 5-dimethylphenyl)-3,5-dihydro-7,8-ethylenedioxy-4 h-2,3-benzodiazepin-4-one (called hereafter 1*g*) as a potent novel growth inhibitor (Parenti et al., 2016). Upon treatment with 1*g*, human leukemia T cells accumulate with a 2N DNA content, suggesting an arrest of cells at the G2/M phase of the cell cycle. In the current study, we have thus evaluated the potential of 1*g* as a novel promising and efficient anti-mitotic drug with a unique effect on microtubule growth.

RESULTS

1*g* arrests cells in mitosis

A previous study has indicated that 1*g* induces an accumulation of Jurkat cells at the G2/M phase of the cell cycle (Parenti et al., 2016). To confirm the effect of 1*g* on the proliferation of transformed human epithelial cells, we followed an asynchronous population of HeLa cells by phase contrast time-lapse microscopy for 20 h (Fig. 1A; Movies 1 and 2). Control cells progressively rounded up to enter mitosis, divided and spread back down over this period of time, increasing the total number of cells. In contrast, cells treated with 1*g* similarly rounded up, but no cell division was observed, suggesting that cells remained arrested in prometaphase and were unable to progress into anaphase and complete their division. This progressive accumulation of rounded cells was observable in a dose-dependent manner with an optimal 1*g* concentration of 2.5 µM (Fig. 1B,C).

To evaluate whether cells treated with 1*g* display a cell division defect, we synchronized HeLa cells at the G2/M transition using the

[1]University of Rennes, CNRS, IGDR (Institut de Génétique et Développement de Rennes) - UMR 6290, 35000 Rennes, France. [2]Department of Life Sciences, University of Modena and Reggio Emilia, 41125 Modena, Italy. [3]Department of Chemical, Biological, Pharmaceutical and Environmental Sciences, University of Messina, 98168 Messina, Italy.

*Authors for correspondence (christelle.benaud@univ-rennes1.fr; lorenzo.corsi@unimore.it; regis.giet@univ-rennes1.fr)

R.G., 0000-0001-9027-5849; L.C., 0000-0002-1667-2624; C.B., 0000-0001-9432-2331

Received 16 September 2019; Accepted 17 February 2020

Journal of Cell Science (2020) 133, jcs239244. doi:10.1242/jcs.239244

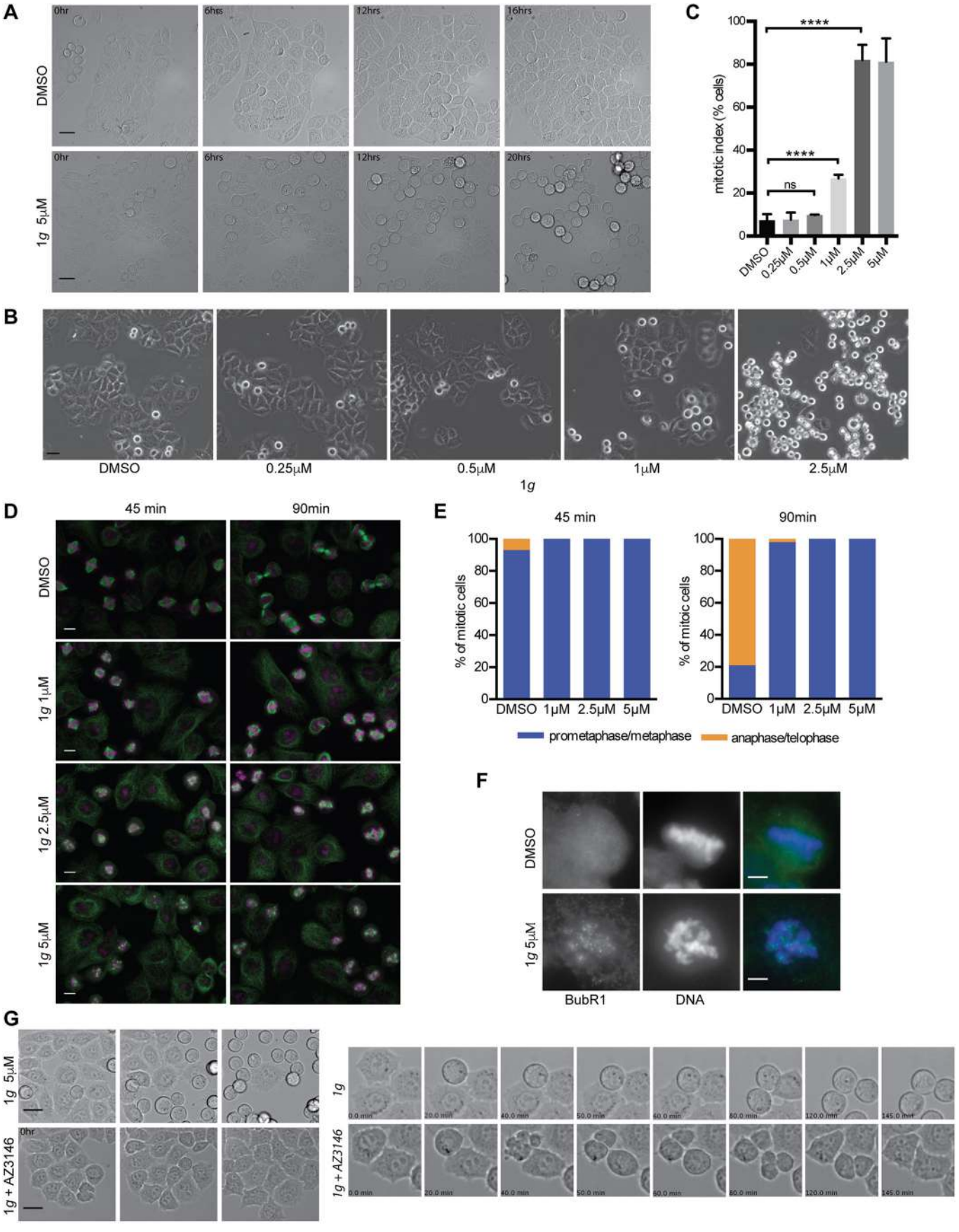

Fig. 1. See next page for legend.

Journal of Cell Science (2020) 133, jcs239244. doi:10.1242/jcs.239244

Fig. 1. 1*g* arrests proliferating cells in prometaphase and activates the spindle assembly checkpoint. (A) Proliferation of HeLa cells treated with DMSO or 1*g* (5 µM) monitored by imaging asynchronous cells for 16 and 20 h. Scale bars: 30 µm. Full sequence is shown in Movies 1 and 2. (B) Dose response effect of 1*g* on cell proliferation. Phase-contrast images of HeLa cells treated with the indicated concentration of 1*g* for 16 h. Scale bar: 30 µm. (C) Mitotic index (% mitotic cells/total cells) of HeLa cells treated with DMSO or the indicated concentration of 1*g* for 16 h (n≥150 cells). Unpaired Student's *t*-test, ****P<0.0001; ns, not significant. Values are mean±s.d. (D) Cells synchronized at the G2/M transition were released in the presence of DMSO or the indicated concentration of 1*g* for 45 min (metaphase in control cells) or 90 min (telophase in control). Cells are stained for α-tubulin in green and DNA in magenta. Scale bars: 10 µm. (E) Quantification of mitotic cell repartition in the different phases of mitosis in presence of increasing concentrations of 1*g* (n≥80 cells). (F) HeLa cells synchronized at the G2/M transition were released in the presence of DMSO or 5 µM 1*g* for 45 min. *Z*-stack projections of cells stained for the presence at the kinetochore of the SAC protein BUBR1 (green) and DNA (blue), with merged images on the right. Scale bars: 5 µm. (G) Activation of the SAC arrests 1*g*-treated cells in prometaphase. Live phase-contrast imaging of proliferating asynchronous HeLa cells treated with 5 µM 1*g* alone or in combination with 2 µM AZ3146. Scale bars: 30 µm. Full sequence is shown in Movies 3 and 4.

CDK1 kinase inhibitor RO3306 (Vassilev, 2006), then released them in the presence of DMSO (control) or 1*g* and followed their progression through mitosis (Fig. 1D,E). Their mitotic stage was defined by staining the cells for tubulin and DNA. As expected, control cells reached the metaphase–anaphase transition within 45 min and 79% of the cells were in telophase at 90 min post-release. In contrast, only 6% of cells treated with 1 µM 1*g* had passed the metaphase–anaphase transition by 90 min and none of the dividing cells exposed to 2.5 µM and 5 µM 1*g* had reached anaphase. Furthermore, dividing cells treated with 2.5 µM and 5 µM 1*g* remained in prometaphase, displaying an abnormal mitotic spindle (Fig. 1D, bottom right panel). Whereas control cells were able to fully congress their chromosomes to the metaphase plate within 45 min, cells treated with 1*g* still displayed major congression defects at 90 min (Fig. 1D,F and Fig. 2B,D). This failure to establish a metaphase plate was associated with the detection of the SAC component BUBR1 on the kinetochore in agreement with an activation of the SAC (Fig. 1F). The drastic increase in the mitotic index (Fig. 1C) of the asynchronous cell population after a 16 h exposure to 1*g* implies that at high drug concentration, cells remain blocked in mitosis (82±5% in 2.5 µM 1*g* versus 7.4±0.81% in DMSO). Instead, the more modest increase in mitotic index (26.8±0.8% in 1 µM 1*g* versus 82.0±5.0% in 2.5 µM 1*g*) when cells were exposed to 1 µM 1*g* suggests that at suboptimal 1*g* concentrations, cells can progress through mitosis but with extensive delay. Indeed, anaphase figures could be observed 4 h post-release in cells treated with 1 µM 1*g*, but not with higher concentrations (data not shown).

To confirm that the accumulation of rounded cells observed in the asynchronous cell population treated with 1*g* (Fig. 1A) was indeed due to activation of the SAC making the cells unable to exit mitosis, HeLa cells were treated with 1*g* alone or in combination with the SAC inhibitor AZ3146 (Tipton et al., 2013), and followed by videomicroscopy. In the presence of AZ3146, 1*g*-treated cells progressively rounded up, but unlike cells treated with 1*g* alone, proceeded through a defective anaphase-telophase and spread back down. It is interesting to note that these cells displayed no cytosolic sign of cell death throughout the 16 h of the treatment with both inhibitors (Fig. 1G; Movies 3 and 4). These data indicate that 1*g* impacts cell proliferation via mitotic arrest and not direct cell death. However, prolonged mitotic arrest has been shown to result in subsequent cell death (Brito and Rieder, 2006; Stanton et al., 2011), explaining the previously described apoptotic effect of the 1*g* compound observed after 48 h of treatment (Parenti et al., 2016). All together, these experiments demonstrate that treatment of proliferating HeLa cells with 1*g* activates the SAC, arresting the cells in prometaphase.

1*g* disrupts formation of the mitotic spindle

The disorganized mitotic spindle observed in 1*g*-treated cells, prompted us to further characterize the dynamics of the mitotic spindle assembly. To that purpose, using spinning-disk microscopy, we imaged live HeLa cells expressing GFP-tubulin after their release from the CDK1 inhibitor-induced G2/M arrest (Fig. 2A,B; Movies 5–7). Control cells treated with DMSO rapidly separated their spindle poles and 100% of the cells formed a bipolar spindle within 15±4 min (Fig. 2C). All cells achieved full chromosome congression into a metaphase plate and progressed into anaphase in an average time of 55±7 min (Fig. 2B,D). When treated with low 1*g* concentrations (1 µM), 90% of the cells formed a bipolar spindle within 28±13 min. However, at 80 min after nuclear envelope breakdown (NEB), 90% of cells treated with 1 µM 1*g* still displayed unaligned chromosomes and thus had not satisfied the SAC (arrowheads in Fig. 2B). At higher 1*g* concentrations (2.5–5 µM), several microtubule nucleation sites could be observed and the microtubule growth from centrosomes was strongly reduced (Fig. 2A, arrowheads). Although clustering of the microtubule asters could be observed, in 70% of the cells exposed to 2.5 µM 1*g* and in 100% of those treated with 5 µM, three asters or more were present and strong chromosome congression defects were observed at 80 min post NEB (Fig. 2B, arrows, D,E). No bipolar mitotic spindles were formed at those concentrations (Fig. 2C). Visualization of the centrosomes, using HeLa cells expressing the centriolar protein centrin-GFP, confirmed that microtubule nucleation emanated from the two centrosomes. However, the additional small asters observed did not contain centrin-GFP, indicating that 1*g* did not trigger centrosome amplification (Fig. 2G). In addition, a decrease of 25% (1 µM 1*g*) and 37% (2 µM 1*g*) in spindle poles distance compared with control cells was observed (Fig. 2F). The defect in centrosome separation was further accentuated at 5 µM, with a 64% decrease in distance between centrosomes in cells treated with 5 µM 1*g* compared with DMSO (Fig. 2H). The formation of shorter microtubules observed in the presence of 1*g* most likely accounts for the reduced centrosome separation, since centrosome separation is a microtubule-dependent process occurring in prophase and prometaphase (Wittmann et al., 2001).

1*g* alters microtubule growth in cells

The dynamic properties of microtubules are crucial for the extensive remodeling of interphase arrays of microtubules into a mitotic bipolar spindle (Desai and Mitchison, 1997). We thus investigated whether 1*g* interferes with microtubule polymerization. We first performed a depolymerization–repolymerization type of assay (Fig. 3A). The microtubule network of interphase cells was depolymerized at 4°C in the presence or absence of 1*g*. We then followed the dynamics of microtubule regrowth as the samples were returned to 37°C. Long newly nucleated microtubules could be observed 5 min after the temperature switch in control cells, and extensive microtubule repolymerization was present after 10 min. Presence of 1*g* did not affect cold-induced depolymerization of microtubules, indicating that 1*g* does not act as a microtubule-stabilizing agent (Fig. 3A, t=0 and G). Indeed, in the presence of

Journal of Cell Science (2020) 133, jcs239244. doi:10.1242/jcs.239244

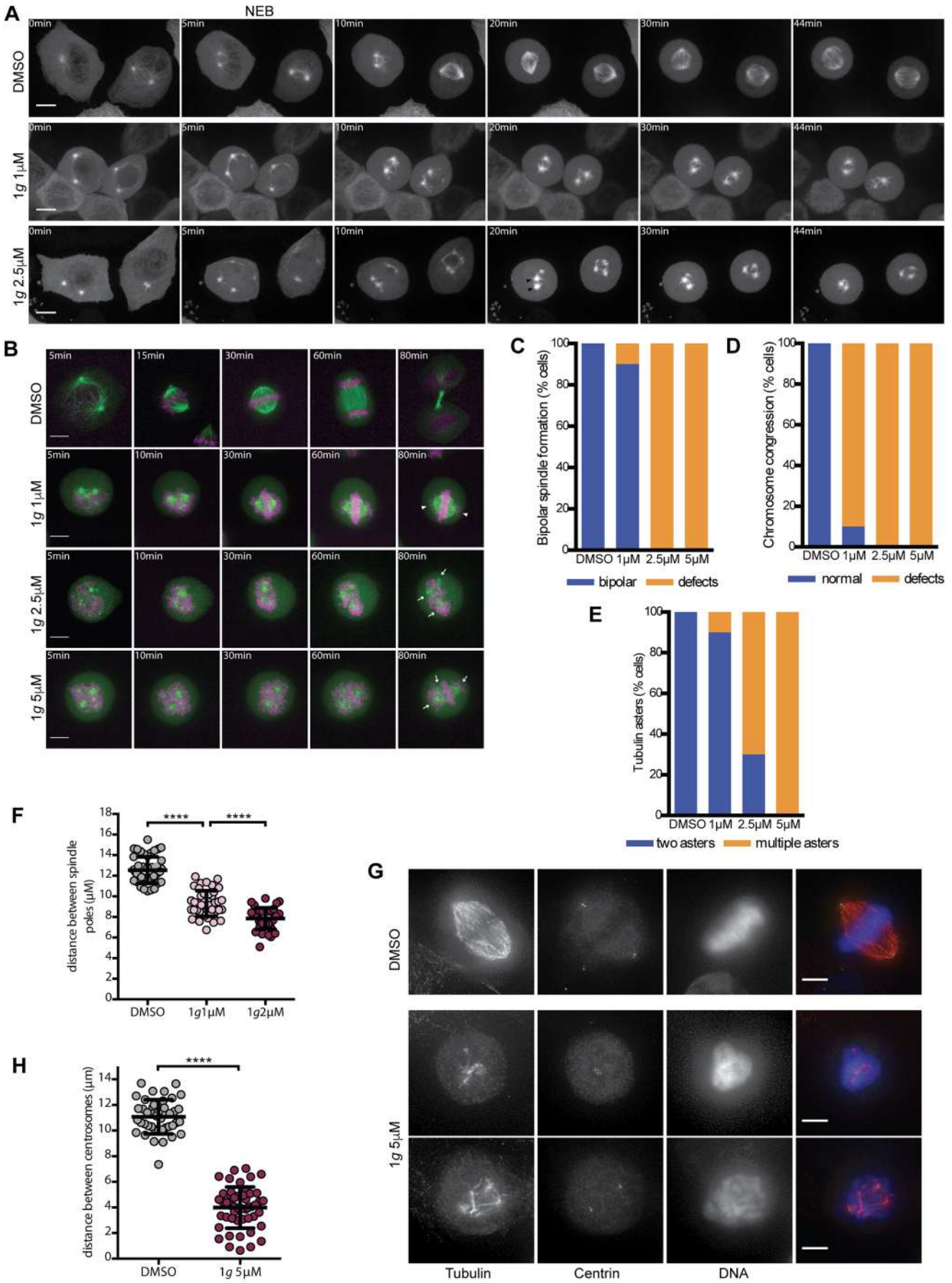

Fig. 2. See next page for legend.

Journal of Cell Science (2020) 133, jcs239244. doi:10.1242/jcs.239244

Fig. 2. 1*g* interferes with mitotic spindle assembly in dividing cells. (A) Spinning-disk images (max projection) of HeLa tubulin-GFP cells undergoing mitosis in presence of DMSO, 1 µM or 2.5 µM 1*g*. Scale bars: 10 µm. Full sequence is shown in Movies 5–7. (B) HeLa cells expressing tubulin-GFP (green) and H2B-mCherry (magenta) imaged for 90 min following G2/M released in presence of DMSO or the indicated concentration of 1*g*. t=0, nuclear envelop breakdown (NEB); arrows indicate microtubule asters and arrowhead unaligned chromosomes. Scale bars: 10 µm. (C) Quantification of cells treated with the indicated concentration of 1*g* forming a bipolar spindle by 80 min. $n\geq15$. (D) Quantification of cells congressing their chromosomes into a metaphase plate by 80 min. $n\geq15$. (E) Quantification of microtubule asters in cells treated with the indicated concentration of 1*g* at t=80 min. $n\geq18$. (F) Analysis of the distance between spindle poles, 45 min after release from G2/M block in cells treated with DMSO or 1 µM and 2 µM of 1*g*. $n\geq40$ cells. (G) HeLa centrin-GFP cells synchronized at the G2/M transition were released for 45 min in the presence of DMSO or 5 µM 1*g* and stained for tubulin (red), GFP (green) and DNA (blue). DeltaVision deconvoluted projections. Scale bars: 5 µm. (H) Analysis of centrosome separation in cells treated with DMSO or 5 µM 1*g*. $n\geq49$ cells. Unpaired Student's *t*-test, ****$P<0.0001$. Bars indicate mean±s.d.

stabilizing agents, such as taxan, cold-resistant microtubule bundles can be detected (Stanton et al., 2011). However, 1*g* markedly slowed down the dynamics of the microtubule network reformation (Fig. 3A, t=5, 10 and 15 min). Only short and fragmented microtubules were observed in 1*g*-treated cells in the first 10 min, and it required 30 min to polymerize a microtubule network equivalent to the one formed after 15 min in control cells.

The growing microtubule plus-end tracking protein (+TIP) EB1 has been commonly used to image microtubule plus-ends and to quantify their dynamics (Matov et al., 2010). To further investigate and quantify the effect of 1*g* on microtubule dynamics, we imaged HeLa cells expressing EB1-GFP by spinning disk confocal microscopy at 1 s time intervals before and immediately after addition of 1*g* or DMSO (Fig. 3B; Movies 8 and 9). In control HeLa cells, measurements of EB1 comet velocity indicated a microtubule growth speed of 16.6±0.83 µm min^{-1}. Whereas addition of DMSO in control cells did not significantly alter microtubule growth speed, 1*g* treatment resulted in a 25% decrease in mean growth rate (from 14.2±0.3 before to 10.6±0.3 µm min^{-1} with 2.5 µM 1*g*) (Fig. 3C,D) without affecting the median growth lifetime. Furthermore, the initial microtubule growth pattern (before treatment, Fig. 3B,C) was recovered shortly after drug removal (washout, Fig. 3B,C) indicating that the action of 1*g* is reversible (15.3±1.1 µm min^{-1} after washout) (Fig. 3B,C; Movies 8 and 9). Treatment with 1*g* did not significantly alter the number of nucleation events (Fig. 3E) or the number or duration of growth pauses (Fig. 3F). In control cells, we could infer a shrinkage rate of 32.9±2.2 µm min^{-1}, which was not statistically different in DMSO-treated cells (34.5 ±1.7 µm min^{-1}). In the presence of 1*g*, no shrinkage events were detected. When tracking EB1 comets, shrinkage can only be inferred when followed by significant EB1-labelled microtubule regrowth (Matov et al., 2010). The absence of detectable shrinkage in the presence of 1*g* could be explained by the fact that the main events occurring were terminal shortenings and shrinkage followed by short or slow growth phases that did not produce detectable EB1 comets within the temporal window analyzed. We thus clearly observed a slowdown in microtubule polymerization in interphase cells. Altogether, these data indicate that 1*g* is able to promote a fast and reversible inhibition of microtubule growth during interphase and mitosis.

To assess whether the 1*g* compound directly targets tubulin polymerization, we tested its impact on microtubule self-assembly *in vitro*. We performed turbidity assays classically used to analyze the effect of drugs or MAPs on microtubule assembly, including microtubule nucleation and elongation (Gallaud et al., 2014) (Fig. 3G). Absorbance at 350 nm, which is directly proportional to the amount of microtubule polymers formed, revealed no significant difference when purified tubulin was incubated in polymerizing buffer at 37°C in the presence of a range of 1*g* concentrations or DMSO. More specifically, we did not observe any effect of the drug on nucleation (same lag-phases at different concentrations), on elongation (sigmoid) phase, or on the plateau of polymerization (total mass of microtubules assembled). In addition, no significant formation of aggregates was detected when the temperature was shifted back to 0°C as the average absorbance returned to the base line for all samples. The absence of significant alteration in tubulin polymer assembly or on formation of aggregates indicates that 1*g* does not interfere with microtubule self-assembly directly.

1*g* interferes with cell division in tissue

During the past decades, *Drosophila melanogaster* has emerged as an interesting model to identify new genes required for cell division as well as for cancer research (Gonzalez, 2013). Therefore, we examined the impact of the compound on neural stem cell (neuroblast) division, in the developing brain of *Drosophila* larvae. Third instar larval brains expressing RFP-α-tubulin and H2A-GFP were dissected and cultured in Schneider medium containing DMSO, or various concentrations of 1*g*. For comparison, we used in parallel 20 µM taxol and 10 µM nocodazole treatments (Fig. 4A; Fig. S1). Control neuroblasts formed bipolar spindles and started to segregate their chromosomes 5.9±0.4 min after the NEB. As expected, following prolonged mitotic arrest, neuroblasts treated with taxol or nocodazole underwent slippage (Fig. S1D,E). In the presence of 1*g*, mitosis duration was significantly increased in a dose-dependent manner (6.1±0.6 min, 8.2±0.6 min and 10.9±3.1 min for 5 µM, 10 µM and 20 µM treatment, respectively) (Fig. 4D), suggesting an activation of the SAC. The delay observed was in the range of that observed in neuroblasts depleted of Msps (15.5±0.8 min, $n=44$) (Fig. S1D), a MAP that has been described to severely disrupt the integrity of the mitotic spindle when downregulated (Cullen et al., 1999). Furthermore, in agreement with SAC activation, 1*g*-treated neuroblasts exhibited dose-dependent mitotic spindle assembly defects (5 µM: 35.3%, 10 µM: 100% of neuroblasts) (Fig. 4B). Lagging chromatids were frequently observed in 31.3% ($n=6/17$) and 68.4% ($n=13/19$) of neuroblasts treated with 10 and 20 µM of 1*g*, respectively (Fig. 4C). In 79% ($n=42$) of cells, we observed the presence of tripolar spindles and the formation of two central spindles (Fig. 4A, 1*g* 8, 9, 13 min, Fig. 4E,F). The outcome of mitosis was variable. Whereas some cells proceed to double cytokinesis, leading to the formation of three daughter cells (Fig. 4A, circled in 1*g* panels), in some instances, regression of the initial double cytokinesis furrow could also be observed. In either case, following defective division 1*g*-treated neuroblast progenies were able to polymerize microtubules from their interphase centrosome (Fig. 4G,H).

DISCUSSION

We show here that the anti-proliferative effect of 1*g* in cancer cell lines observed previously (Parenti et al., 2016) is caused by interference with microtubule polymerization and defective mitotic spindle assembly, leading to SAC activation. Of note, the 1*g* concentrations used in cell treatments (5 µM or less) are 20 times less than the K_d for the AMPA receptor (K_d>100 µM; Micale et al.,

Journal of Cell Science (2020) 133, jcs239244. doi:10.1242/jcs.239244

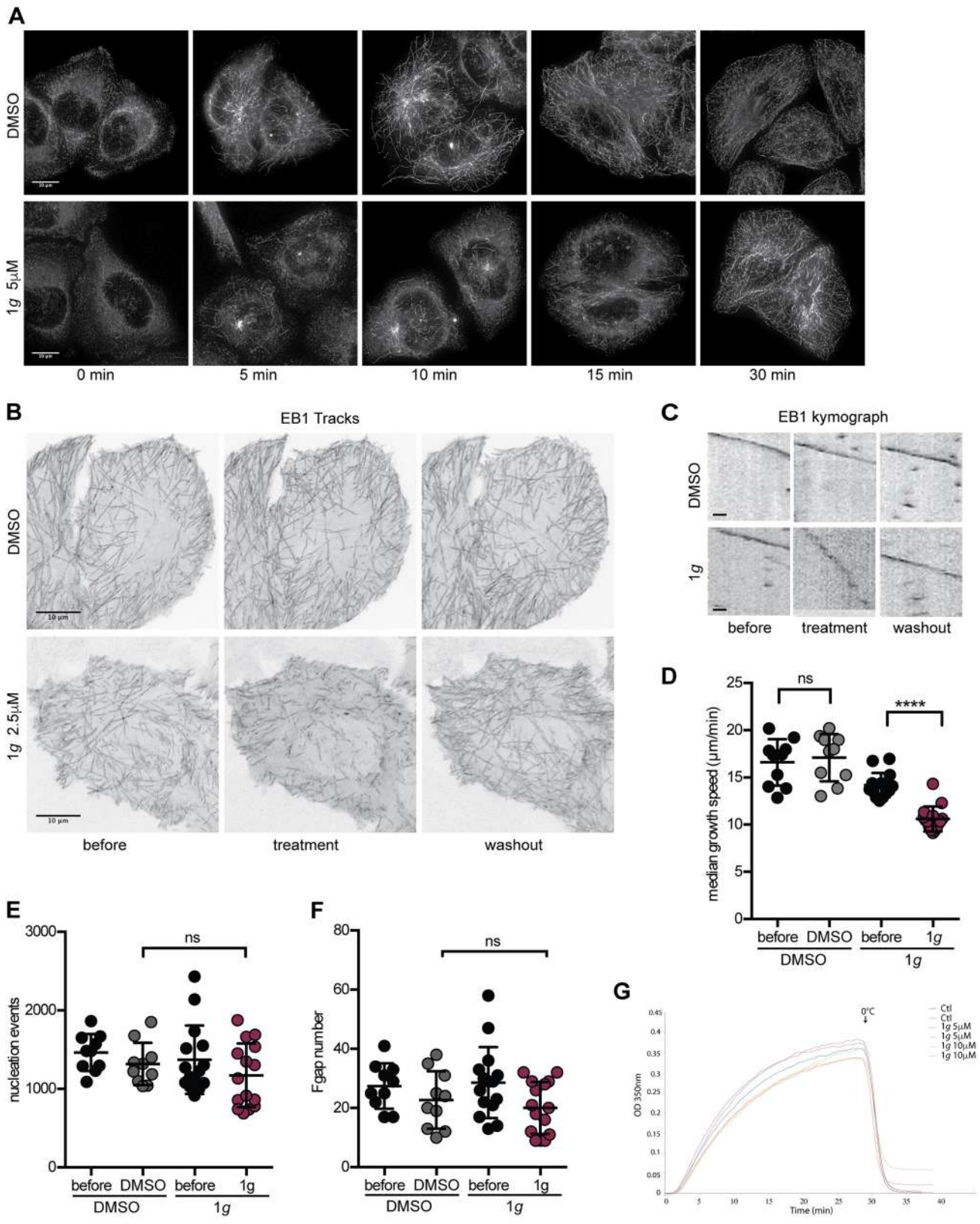

Fig. 3. See next page for legend.

2008), indicating that the strong effects of 1*g* on cell division are independent of the AMPA receptor signaling pathway.

Our *in vitro* assays with pure tubulin indicate that 1*g* does not directly target the intrinsic microtubule polymerization. When 1*g* was used *in vitro* within cells or *in vivo*, we did not observe the massive effects on the microtubule cytoskeleton that are triggered with microtubule binding agents such as taxol or nocodazole. Instead, under 1*g* treatment, the overall architecture of the HeLa cell

Journal of Cell Science (2020) 133, jcs239244. doi:10.1242/jcs.239244

Fig. 3. 1*g* alters microtubule growth in cells. (A) Microtubules of HeLa cells treated with DMSO or 5 µM 1*g* were depolymerized at 4°C (t=0) and allowed to repolymerize by switching back the cells to 37°C for the indicated times. *Z*-stack projection images of cells stained for α-tubulin. (B) Spinning-disk time-lapse images of HeLa EB1-GFP cells (1 image/s) before treatment, in presence of DMSO or 2.5 µM 1*g*, and after washing out the drug (see also Movie 8 for control and Movie 9 for 1*g*). Time projection of EB1-GFP over 1 min is presented for the different conditions. (C) Kymograph [time (s) vs distance[representations of the EB1 tracks over 1 min. Scale bars: 1 µm. Quantification of EB1 comet velocity (D) nucleation events (E) and inferred number of pauses (F). For each condition $n \geq 700$ tracks in 10 (control) to 15 (1*g*) independent measurements. Unpaired Student's *t*-test, ****$P<0.0001$; ns, not significant. Bars indicate mean±s.d. (G) *In vitro* microtubule polymerization assay. DMSO (control) or 5 and 10 µM 1*g* was added to purified tubulin in polymerization buffer at 4°C. The formation of microtubule polymers was monitored by the absorbance at 350 nm as the temperature was increased to 35°C. Formation of stable aggregates are visualized as temperature is shifted back to 4°C.

interphase microtubule network remained intact. Moreover, *Drosophila* neuroblasts were still able to nucleate *de novo* microtubules from the daughter centrosome following division. As cells proceed from interphase to mitosis, a 10-fold increase in the turnover rate of microtubules is required for the reorganization of the microtubule network into a mitotic spindle and for the capture of chromosomes (Desai and Mitchison, 1997; Prosser and Pelletier, 2017). This change in microtubule turnover rate implies that a drug that moderately impedes microtubule dynamics in interphase would be expected to trigger more drastic effects on mitotic microtubules. Indeed, the main effect of 1*g* was observed during cell division in fly brain neuroblasts and in HeLa cells.

In both systems exposed to 1*g*, SAC activation was observed, resulting either in mitotic delay in fly neuroblasts or in mitotic arrest in mammalian cells. Whereas neuroblasts treated with taxol or nocodazole (which severely impair spindle assembly) remained arrested and underwent mitotic slippage, the mitotic delay in fly neuroblasts treated with 1*g*, did not exceed three times the duration of cell division. The presence of kinetochores not attached to microtubules of the mitotic spindle causes SAC activation and mitotic arrest. In 1*g*-treated neuroblasts, the observation of a mitotic delay rather than a mitotic arrest, suggests that despite displaying a tripolar shape, the spindle microtubules still manage to grow and correctly attach kinetochores. However, the altered microtubule growth results in a time delay to perform that task and satisfy the SAC. In contrast, HeLa cells remained arrested following 1*g* treatment. The difference in genome size could account for this difference in the 1*g* drug response. Fly cells harbor only four chromosomes, making it easier to achieve kinetochore attachment under defective MT polymerization and thus satisfy the SAC and exit mitosis. By contrast, SAC satisfaction is likely more problematic for HeLa cells that require the correct attachment of 70–82 chromosomes (Landry et al., 2013).

Nevertheless, the mitotic phenotypes are similar between neuroblasts and HeLa cells: the centrosomal microtubule asters are present, but they only nucleate short microtubules. Moreover, additional microtubule asters are detected, which fail to coalesce into a bipolar structure. This inability to form a bipolar spindle suggests that not only is the growth of MT altered, but the structure of the metaphase spindle, such as the organization/bundling of the interpolar microtubules, is also affected. Altogether, our results support the hypothesis that 1*g* targets a MAP involved in the regulation of microtubule growth during interphase and mitosis, which is essential for mitotic spindle assembly. The similarities in the mitotic phenotypes observed in HeLa cells and fly neural stem cells indicate that the 1*g* target and its functional motifs are likely to be conserved between humans and flies. Further studies will be needed to identify the direct cellular target of 1*g* in order to obtain further insight on its mechanism of action.

Microtubule-targeting agents are widely used in chemotherapy, but their lack of specificity for dividing tumor cells is a limitation. Indeed, their toxicity for the neural, immunological and gastric systems, due to their profound effect on interphase microtubules functions as well as tumor resistance, foster a need for development of new agents (Dumontet and Jordan, 2010; Stanton et al., 2011). The targets of choice are cellular microtubule regulators that modulate microtubule dynamics and organization specifically in proliferating cells. As discussed above the 1*g* compound may comply with the requirement of new pharmaceutical compounds with a more specific mode of action.

MATERIALS AND METHODS

Cell culture

HeLa Kyoto cells were grown in Dulbecco's modified Eagle's medium Glutamax (Gibco) supplemented with 10% fetal calf serum (PAA), 100 U/ml penicillin and 100 µg/ml streptomycin. For synchronization experiments, cells were treated for 16 h with 5 µM RO-3306 to arrest cells in G2/M, cells were then washed in complete medium and released for the indicated times. pEGFP-Tub (BD Biosciences), pGFP- EB1 (gift from Philippe Chavrier, Institut Curie, France) and were used to generate tubulin-GFP and EB1-GFP HeLa stable cell lines, respectively.

Small-molecule inhibitors

1*g* was synthesized by Roberta Ettari (University of Messina, Italy) (Parenti et al., 2016) and its purity verified by ^{1}H- NMR and ^{13}C-NMR. Absence of contaminants was also subsequently confirmed by HPLS-MS-MS. 1*g* was dissolved in DMSO at a stock concentration of 50 mM. Further dilutions were performed in tissue culture medium. DMSO control treatment is equivalent to the amount of DMSO present in the highest 1*g* treatment concentration used in the experiment. The final DMSO concentrations in the assays were therefore less or equal to 0.01% in HeLa cell experiments and 0.04% for *Drosophila* tissue experiments. The Mps1 inhibitor AZ3146 was from Calbiochem, the CDK1 inhibitor RO-3306 was from Merck, taxol and nocodazole were from Sigma-Aldrich.

Antibodies, immunoblotting and immunofluorescence

The following commercial antibodies were used: α-tubulin (clone YL1/2, Millipore; 1:1000), anti-BUBRI (clone 9, BD Biosciences; 1:500), anti-GFP (clone7.1 and 13.1, Roche; 1:1000), anti-phospho histone H3 (clone CMA312, Millipore; 1:1000). DNA was stained with Hoechst 33342 or To-Pro-3 iodide (Invitrogen). For microtubule immunofluorescence staining, cells were grown on glass coverslips and fixed with methanol at −20°C (tubulin). For BubR1 staining, cells were first permeabilized with 0.5% Triton in PHEM (60 mM PIPES, 25 mM HEPES, 10 mM EGTA, 4 mM $MgSO_4$•$7H_2O$) for 5 min at room temperature and then fixed with paraformaldehyde in PHEM for 10 min. Antibody staining was then performed as described previously (Benaud et al., 2004). Brain from wandering third instar larvae were dissected and maintained in 100 µl of Schneider medium supplemented with DMSO or 20 µM 1*g* for 1 h at 25°C before fixation and immunostaining, as described previously (Gallaud et al., 2014).

Drosophila stocks

Flies were maintained under standard conditions at 25°C. w^{1118} flies were used as controls for immunostaining experiments. Flies expressing H2A-GFP (Clarkson and Saint, 1999) and the recombinant Insc-Gal4, UAS-mCherry-α-tubulin as well as *UAS-ChRFP::Tubulin* (BDSC 25774) and *Insc-Gal4* (BDSC 8751) were obtained from the Bloomington *Drosophila* Stock Center (Indiana University, #5941 and #25773, respectively). The flies ubiquitously expressing tubulin tagged with RFP (RFP-tub) was a gift from Renata Basto (Institut Curie, Paris, France). The cell membrane marker Ubi-PH(PLCγ)-GFP (Gervais et al., 2008) was a gift

Journal of Cell Science (2020) 133, jcs239244. doi:10.1242/jcs.239244

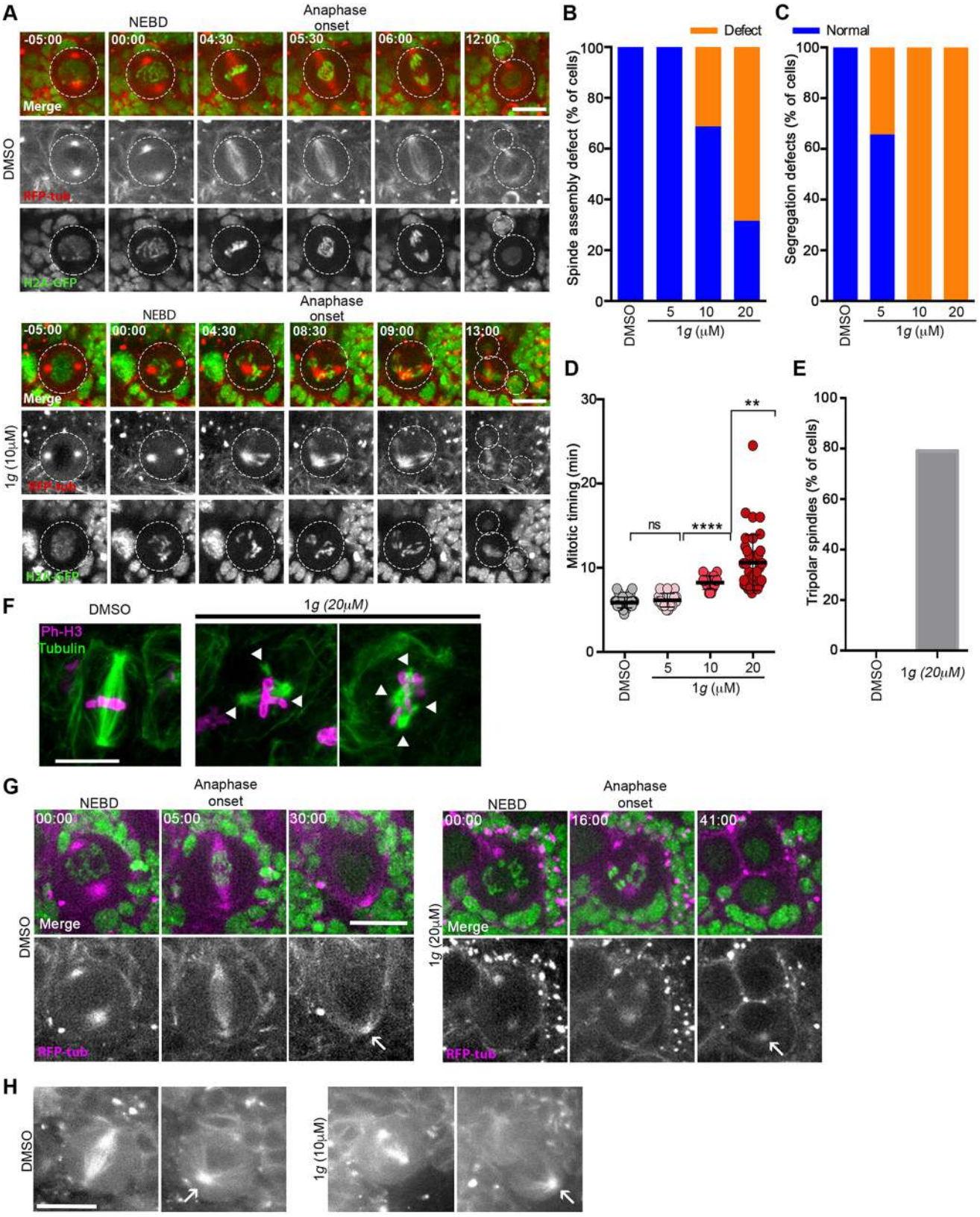

Fig. 4. See next page for legend.

from Antoine Guichet (Institut Jaccques Monod, Paris, France). The Msps RNAi line (ref. GD21982) was purchased from the Vienna *Drosophila* RNAi Center. The knockdown of *Msps* in central brain neuroblasts was driven by Insc-Gal4.

Live-cell imaging and microscopy

For live imaging, *Drosophila* brains expressing H2A-GFP and mCherry-α-tubulin were dissected in Schneider's *Drosophila* medium containing 10% FCS. Following 10 min pre-incubation with DMSO or the indicated

Fig. 4. Effect of 1*g* on *Drosophila* neuroblast proliferation. Dividing neural stem cells of *Drosophila* brains expressing tubulin-RFP and histone H2B-GFP imaged by spinning-disk confocal microscopy. (A) Selected frames of dividing *Drosophila* larval neuroblasts incubated with DMSO or 1*g*. Time 00:00 (min: s)=NEB. Dotted circle outlines the neuroblast cell contour (t=–05:00–t=09:00) and the neuroblast progeny (t=12:00/13:00): neuroblast (large circle) and ganglion mother cell GMC (small circle). Scale bars: 10 µm. (B) Analysis of the percentage of mitotic spindle assembly defects in neuroblasts treated with DMSO or 1*g*. $n \geq 17$ cells for each condition. (C) Analysis of chromosome segregation defects corresponding to lagging chromosomes in DMSO- and 1*g*-treated brains. $n \geq 17$ cells. (D) Analysis of mitosis duration measured from NEB to anaphase onset in neuroblasts exposed to DMSO (05:87±0.1, n=43), 5 µM (06:14±0.19, n=17), 10 µM (08:24±0.19, n=17), 20 µM (10:60±0.5, n=42) 1*g* (time in min:s). $^{**}P<0.0012$; $^{***}P<1.3\times10^{-4}$ (Wilcoxon test); ns, not significant. Bars indicate mean±s.d. (E) Analysis of the frequency of formation of tripolar spindle in neuroblast treated with DMSO (0%, n=44) or 20 µM 1*g* (87%, n=42). (F) *Z*-stack image of prometaphase neuroblasts incubated for 1 h in DMSO or 1*g* and stained for α-tubulin (green) and DNA (magenta). Arrowheads indicate tripolar asters. Scale bar: 10 µm. (G,H) Selected frames illustrating interphase aster reformation following mitosis of *Drosophila* larval neuroblasts incubated with DMSO or 1*g*. Arrows indicate interphase aster. Scale bars: 10 µm.

concentration of chemical compounds, isolated brains were loaded and mounted on stainless steel slides. The preparations were sealed with mineral oil (Sigma-Aldrich) as previously described (Gallaud et al., 2014). HeLa cells were grown in Lab-Tek I chambered coverglasses (Nunc). Bright-field images of asynchronous dividing HeLa cells were acquired every 5 min with a 20× objective on a DMRIBE inverted microscope (Leica) equipped with CO_2 heated incubator chamber and a CoolSNAP ES BW camera (Roper Scientific). Live fluorescent images were acquired on a spinning disk microscope using a Plan Apo 60×/1.4 NA objective on an Eclipse Ti-E microscope (Nikon) equipped with a spinning disk (CSU-X1; Yokogawa), a thermostatic chamber (Life Imaging Service), Z Piezo stage (Marzhauser), and a charge-coupled device camera (CoolSNAP HQ2; Roper Scientific). *Drosophila* live images were alternatively acquired with a spinning-disk system consisting of a DMi8 microscope (Leica) equipped with a 63×/1.4NA oil objective, a CSU-X1 spinning-disk unit (Yokogawa) and an Evolve EMCCD camera (Photometrics). The microscope was controlled by the Inscoper Imaging Suite and the dedicated software (Inscoper).

For HeLa cells, time-lapse tubulin-GFP images were acquired every 1 min for the 45 min time lapse or every 5 min for the 90 min time lapse, and EB1GFP comets every 0.5 s using Metamorph Software (Universal imaging). For *Drosophila* neuroblasts, Z-series were acquired every 30 or 60 s. Immunofluorescence images of fixed samples were acquired with an SP5 confocal microscope (Leica) or with an API DeltaVision microscope equipped with a coolSnapHQ camera (Princeton instruments) using the SoftWorX software. Image acquisition was coupled to deconvolution when indicated. Images were processed and measurements performed using Fiji software (http://fiji.sc/). Analysis of EB1 comets was performed using the MATLAB-based open source u-track particle tracking (version 2.0) software (Danuser Lab, UT Southwern Medical Center).

Turbidimetry assay

Commercial lyophilized tubulin (PurSolutions, Nashville, USA) was reconstituted at 500 µM in distilled water according to the manufacturer's instructions. Tubulin was diluted at 50 µM in 10% glycerol, 1 mM GTP, 0.02% DMSO in BRB80 buffer (80 mM K-Pipes, 1 mM EGTA, 1 mM $MgCl_2$, pH 6.8 with KOH), and in the presence of 0 µM, 5 µM or 10 µM 1*g*. Control samples contained the same amount of DMSO as 1*g* samples. Suspensions were centrifuged at 33,000 ***g*** at 4°C for 5 min before polymerization. Samples were transferred into 100 µl quartz cuvettes (Hellma), and measurements at 350 nm were performed in a UVIKON XS spectrophotometer maintained at 35°C to stimulate tubulin polymerization. After 30 min of polymerization, depolymerization was induced by a cold temperature shift at 4°C to assess the presence of aggregates.

Acknowledgements

The imaging work was performed on the platform MRic-Photonics (BIOSIT, Université Rennes1). We thank Thibault Courtheoux for his help with the use of plus-tip tracker software and Laurent Richard-Parpaillon for critical discussion.

Competing interests

The content of this paper is included in a current patent application.

Author contributions

Conceptualization: D.C., R.G., L.C., C.B.; Methodology: S.K.; Investigation: V.P., M.M., E.G., A.T.; Resources: R.E.; Writing - original draft: C.B.; Writing - review & editing: R.G.; Project administration: C.B.

Funding

V.P. was financed by the Erasmus+ program. C.B. is supported by INSERM and La Ligue Contre le Cancer (Grand Ouest-Bretagne); D.C. by the Agence Nationale de la Recherche (ANR-16-CE11-0017-01) ; L.C. by Fondazione di Vignola 2014; M.M. and A.T. by La Ligue Régionale Contre le Cancer (Grand Ouest-Bretagne), Region Bretagne; E.G. by La foundation pour la Recherche Médicale (DEQ20170336742); R.G. by La Ligue and Fondation ARC pour la Recherche sur le Cancer. This work was supported by the Centre National de la Recherche Scientifique, the University of Rennes 1.

Supplementary information

Supplementary information available online at
http://jcs.biologists.org/lookup/doi/10.1242/jcs.239244.supplemental

Peer review history

The peer review history is available online at https://jcs.biologists.org/lookup/doi/10.1242/jcs.239244.reviewer-comments.pdf

References

Argyriou, A. A., Bruna, J., Marmiroli, P. and Cavaletti, G. (2012). Chemotherapy-induced peripheral neurotoxicity (CIPN): an update. *Crit. Rev. Oncol. Hematol.* **82**, 51-77. doi:10.1016/j.critrevonc.2011.04.012

Benaud, C., Gentil, B. J., Assard, N., Court, M., Garin, J., Delphin, C. and Baudier, J. (2004). AHNAK interaction with the annexin 2/S100A10 complex regulates cell membrane cytoarchitecture. *J. Cell Biol.* **164**, 133-144. doi:10.1083/jcb.200307098

Brito, D. A. and Rieder, C. L. (2006). Mitotic checkpoint slippage in humans occurs via cyclin B destruction in the presence of an active checkpoint. *Curr. Biol.* **16**, 1194-1200. doi:10.1016/j.cub.2006.04.043

Clarkson, M. and Saint, R. (1999). A His2AvDGFP fusion gene complements a lethal His2AvD mutant allele and provides an in vivo marker for Drosophila chromosome behavior. *DNA Cell Biol.* **18**, 457-462. doi:10.1089/104454999315178

Cullen, C. F., Deák, P., Glover, D. M. and Ohkura, H. (1999). mini spindles: a gene encoding a conserved microtubule-associated protein required for the integrity of the mitotic spindle in Drosophila. *J. Cell Biol.* **146**, 1005-1018. doi:10.1083/jcb.146.5.1005

Desai, A. and Mitchison, T. J. (1997). Microtubule polymerization dynamics. *Annu. Rev. Cell Dev. Biol.* **13**, 83-117. doi:10.1146/annurev.cellbio.13.1.83

Dumontet, C. and Jordan, M. A. (2010). Microtubule-binding agents: a dynamic field of cancer therapeutics. *Nat. Rev. Drug Discov.* **9**, 790-803. doi:10.1038/nrd3253

Gallaud, E., Caous, R., Pascal, A., Bazile, F., Gagné, J.-P., Huet, S., Poirier, G. G., Chrétien, D., Richard-Parpaillon, L. and Giet, R. (2014). Ensconsin/Map7 promotes microtubule growth and centrosome separation in Drosophila neural stem cells. *J. Cell Biol.* **204**, 1111-1121. doi:10.1083/jcb.201311094

Gervais, L., Claret, S., Januschke, J., Roth, S. and Guichet, A. (2008). PIP5K-dependent production of PIP2 sustains microtubule organization to establish polarized transport in the Drosophila oocyte. *Development* **135**, 3829-3838. doi:10.1242/dev.029009

Gonzalez, C. (2013). Drosophila melanogaster: a model and a tool to investigate malignancy and identify new therapeutics. *Nat. Rev. Cancer* **13**, 172-183. doi:10.1038/nrc3461

Janssen, A. and Medema, R. H. (2011). Mitosis as an anti-cancer target. *Oncogene* **30**, 2799-2809. doi:10.1038/onc.2011.30

Kavallaris, M. (2010). Microtubules and resistanace to tubulin-binding agents. *Nat. Rev. Cancer* **10**, 194-204. doi:10.1038/nrc2803

Khodjakov, A. and Rieder, C. L. (2009). The nature of cell-cycle checkpoints: facts and fallacies. *J. Biol.* **8**, 88. doi:10.1186/jbiol195

Landry, J. J. M., Pyl, P. T., Rausch, T., Zichner, T., Tekkedil, M. M., Stütz, A. M., Jauch, A., Aiyar, R. S., Pau, G., Delhomme, N. et al. (2013). The genomic and transcriptomic landscape of a HeLa cell line. *G3* **3**, 1213-1224. doi:10.1534/g3.113.005777

Matov, A., Applegate, K., Kumar, P., Thoma, C., Krek, W., Danuser, G. and Wittmann, T. (2010). Analysis of microtubule dynamic instability using a plus-end growth marker. *Nat. Methods* **7**, 761-768. doi:10.1038/nmeth.1493

Micale, N., Colleoni, S., Postorino, G., Pellicanò, A., Zappalà, M., Lazzaro, J., Diana, V., Cagnotto, A., Mennini, T. and Grasso, S. (2008). Structure-activity study of 2,3-benzodiazepin-4-ones noncompetitive AMPAR antagonists: identification of the 1-(4-amino-3-methylphenyl)-3,5-dihydro-7,8-ethylenedioxy-

4H-2,3-benzodiazepin-4-o ne as neuroprotective agent. *Bioorg. Med. Chem.* **16**, 2200-2211. doi:10.1016/j.bmc.2007.11.080

Mitchison, T. and Kirschner, M. (1984). Dynamic instability of microtubule growth. *Nature* **312**, 237-242. doi:10.1038/312237a0

Parenti, S., Casagrande, G., Montanari, M., Espahbodinia, M., Ettari, R., Grande, A. and Corsi, L. (2016). A novel 2,3-benzodiazepine-4-one derivative AMPA antagonist inhibits G2/M transition and induces apoptosis in human leukemia Jurkat T cell line. *Life Sci.* **152**, 117-125. doi:10.1016/j.lfs.2016.03.051

Prosser, S. L. and Pelletier, L. (2017). Mitotic spindle assembly in animal cells: a fine balancing act. *Nat. Rev. Mol. Cell Biol.* **18**, 187-201. doi:10.1038/nrm.2016.162

Stanton, R. A., Gernert, K. M., Nettles, J. H. and Aneja, R. (2011). Drugs that target dynamic microtubules: a new molecular perspective. *Med. Res. Rev.* **31**, 443-481. doi:10.1002/med.20242

Stepulak, A., Rola, R., Polberg, K. and Ikonomidou, C. (2014). Glutamate and its receptors in cancer. *J. Neural Transm.* **121**, 933-944. doi:10.1007/s00702-014-1182-6

Tipton, A. R., Ji, W., Sturt-Gillespie, B., Bekier, M. E., II, Wang, K., Taylor, W. R. and Liu, S.-T. (2013). Monopolar spindle 1 (MPS1) kinase promotes production of closed MAD2 (C-MAD2) conformer and assembly of the mitotic checkpoint complex. *J. Biol. Chem.* **288**, 35149-35158. doi:10.1074/jbc.M113.522375

Vassilev, L. T. (2006). Cell cycle synchronization at the G_2/M phase border by reversible inhibition of CDK1. *Cell Cycle* **5**, 2555-2556. doi:10.4161/cc.5.22.3463

Wittmann, T., Hyman, A. and Desai, A. (2001). The spindle: a dynamic assembly of microtubules and motors. *Nat. Cell Biol.* **3**, E28-E34. doi:10.1038/35050669